
Detecting Out-of-Distribution Inputs to Deep Generative Models Using a Test for Typicality

Eric Nalisnick*, Akihiro Matsukawa, Yee Whye Teh, Balaji Lakshminarayanan*

DeepMind

{enalisnick, amatsukawa, ywteh, balajiln}@google.com

Abstract

Recent work has shown that deep generative models can assign higher likelihood to out-of-distribution data sets than to their training data [26, 8]. We posit that this phenomenon is caused by a mismatch between the model’s typical set and its areas of high probability density. In-distribution inputs should reside in the former but not necessarily in the latter, as previous work has presumed [6]. To determine whether or not inputs reside in the typical set, we propose a statistically principled, easy-to-implement test using the empirical distribution of model likelihoods. The test is model agnostic and widely applicable, only requiring that the likelihood can be computed or closely approximated. We report experiments showing that our procedure can successfully detect the out-of-distribution sets in several of the challenging cases reported by Nalisnick et al. [26].

1 Introduction

Recent work [26, 8, 32, 19, 34] has shown that a variety of types of deep generative models fail to distinguish training data from out-of-distribution (OOD) inputs according to the model likelihood. This phenomenon occurs not only when the inputs are similar but also when they have dramatically different underlying semantics. For instance, *Glow* [22], a state-of-the-art normalizing flow, trained on CIFAR-10 will assign a higher likelihood to SVHN than to its CIFAR-10 training data [26, 8]. This result is surprising since CIFAR-10 contains images of frogs, horses, ships, trucks, etc. and SVHN contains house numbers. A human would be very unlikely to confuse the two sets. These findings are also troubling from an algorithmic standpoint since higher OOD likelihoods break previously proposed methods for classifier validation [6, 10]. For example, Bishop [6] proposes training a density estimator on the input features to a classifier, and at test time, new inputs are rejected if they fail to have sufficiently high density. In the CIFAR-10 vs SVHN case described above, this methodology would fail to reject any SVHN inputs, allowing them to be passed to the CIFAR-10 classifier even though its predictions would be nonsensical.

We conjecture that these high OOD likelihoods are evidence of the phenomenon of *typicality*. Due to concentration of measure, samples from a generative model will reside in what is known as the *typical set* [11]. However, *regions of high probability density may not necessarily overlap with the typical set*. For example, consider a d -dimensional isotropic Gaussian. Its highest density region is at its mode (also the mean) but the typical set resides at a distance of \sqrt{d} from the mode [39]. Thus we have the somewhat unintuitive result that a point near the mode will have high likelihood while being extremely unlikely to be sampled from the model. We believe that deep generative models exhibit a similar phenomenon since, to return to the CIFAR-10 vs SVHN example, Nalisnick et al. [26] showed that sampling from the model trained on CIFAR-10 never generates SVHN-looking images despite SVHN having higher likelihood. Based on this insight, *we propose that OOD detection should be done by checking if an input resides in the model’s typical set, not just in a region of high density*.

*Corresponding authors.

Unfortunately, it is impossible to analytically derive the regions of typicality for the vast majority of deep generative models. To define a widely applicable and scalable OOD-detection algorithm, we formulate Shannon [33]’s entropy-based definition of typicality into a statistical hypothesis test. To ensure that the test is robust even in the low-data regime, we employ a bootstrap procedure [16] to set the OOD-decision threshold. In the experiments, we demonstrate that our detection procedure succeeds in many of the challenging cases presented by Nalisnick et al. [26]. In addition to these successes, we also discuss failure modes that reveal drastic variability in OOD detection for the same data set pairs under different generative models. We highlight these cases to inspire future work. In summary, our contributions are:

- A novel formulation of Shannon [33]’s definition of typicality into a statistical test. Furthermore, we translate the test into a practical and robust OOD-detection algorithm by obtaining a bootstrap confidence interval from validation data.
- Experiments demonstrating that our OOD test is successful in several of the challenging cases put forward by Nalisnick et al. [26].
- Observations showing that for some model-data combinations, the empirical distribution of OOD likelihoods *nearly matches* that of the in-distribution likelihoods. This represents a limitation for our test and highlights a fundamental obstacle for essentially all likelihood-based methods.

2 Preliminaries

We begin by establishing notation, reviewing the necessary background material, and defining the setting of interest. We denote matrices with upper-case and bold letters (e.g. \mathbf{X}), vectors with lower-case and bold (e.g. \mathbf{x}), and scalars with lower-case and no bolding (e.g. x).

2.1 Typical Sets

The *typical set* of a probability distribution is the set whose elements have an information content sufficiently close to that of the expected information [33]. A formal definition follows.

Definition 2.1. ϵ -Typical Set [11] *For a distribution $p(\mathbf{x})$ with support $\mathbf{x} \in \mathcal{X}$, the ϵ -typical set $\mathcal{A}_\epsilon^N[p(\mathbf{x})] \in \mathcal{X}^N$ is comprised of all N -length sequences that satisfy*

$$\mathbb{H}[p(\mathbf{x})] - \epsilon \leq \frac{-1}{N} \log p(\mathbf{x}_1, \dots, \mathbf{x}_N) \leq \mathbb{H}[p(\mathbf{x})] + \epsilon$$

where $\mathbb{H}[p(\mathbf{x})] = \int_{\mathcal{X}} p(\mathbf{x})[-\log p(\mathbf{x})]d\mathbf{x}$ and $\epsilon \in \mathbb{R}^+$ is a small constant.

\mathcal{A}_ϵ^N depends on both ϵ and N , and altering these values will decrease or increase the cardinality of the set. When the joint density in Definition 2.1 factorizes, we can write:

$$\mathbb{H}[p(\mathbf{x})] - \epsilon \leq \frac{-1}{N} \sum_{n=1}^N \log p(\mathbf{x}_n) \leq \mathbb{H}[p(\mathbf{x})] + \epsilon. \quad (1)$$

This is the definition we will use from here forward as we assume both training data and samples from our generative model are i.i.d. In this factorized form, we can now interpret the middle quantity as an N -sample empirical entropy: $-1/N \sum_{n=1}^N \log p(\mathbf{x}_n) = \hat{\mathbb{H}}^N[p(\mathbf{x})]$. The *asymptotic equipartition property* (AEP) [11] states that this estimate will converge (in probability) to the true entropy as $N \rightarrow \infty$. The property of most consequence for our application is that the typical set has probability nearly 1 [11] and therefore is a compact summary of what we expect to be generated by $p(\mathbf{x})$.

To give a concrete example, an isotropic Gaussian’s typical set is an annulus with a radius of $\sigma\sqrt{d}$ and with a width of $O(\sigma d^{1/4})$ [39]. Figure 1(a) illustrates this annulus for a Gaussian centered on the all gray image (pixel value 128). We show that samples from this model never resemble the all gray image despite it having the highest probability density, and this is due to them lying on this outer shell. In Figure 1(b) we visualize the mathematics that give rise to the typical set. The red line denotes the probability density, the black line the volume of the space, and the gray-shaded area the typical set. The typical set arises due to probability (mass) being the product of density and volume.

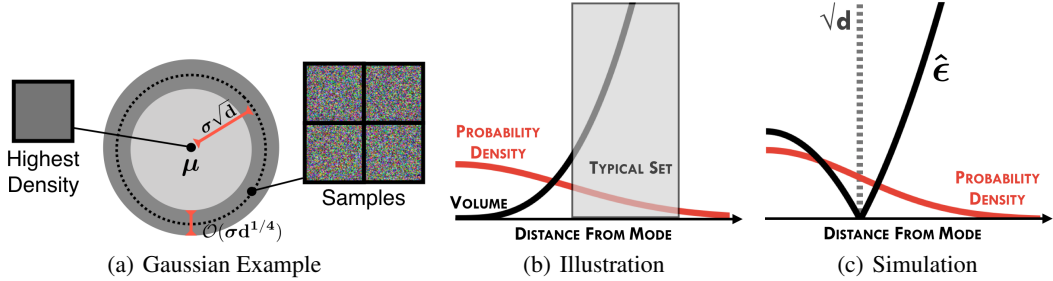


Figure 1: *Typical Sets*. Subfigure (a) shows the example of a Gaussian with its mean located at the high-dimensional all-gray image. Subfigure (b) shows how the typical set arises due to the nature of high-dimensional integration. The figure is inspired by Betancourt [5]’s similar illustration. Subfigure (c) shows our proposed method (Equation 6, higher $\hat{\epsilon}$ implies OOD) applied to a Gaussian simulation. The values have been re-scaled for purposes of visualization.

2.2 Setting of Interest

Assume we have a data set of interest $\mathbf{X} = \{\mathbf{x}_1, \dots, \mathbf{x}_N\}$ and that this data set was drawn from p^* , which is unknown and inaccessible except through \mathbf{X} . Moreover, we assume that N is sufficiently large to enable training a high-capacity deep generative model. We also assume that at test time we will be presented with an M -sized *batch* of observations $\tilde{\mathbf{X}} = \{\tilde{\mathbf{x}}_1, \dots, \tilde{\mathbf{x}}_M\}$ ($M \geq 1$). We desire to determine if $\tilde{\mathbf{X}}$ was sampled (i.i.d.) from the same distribution as \mathbf{X} (i.e. $\tilde{\mathbf{x}}_m \sim p^*$) or from some other distribution $q \neq p^*$. This is roughly the same setting considered by most work on classifier validation with a probabilistic model [6]. That is, we want to use a generative model of the input features to restrict access to a discriminative model deployed in a user-facing system.

It is important to emphasize the differences between this problem definition and the general task of anomaly detection [7, 28]. Anomaly detection aims to discover inputs that are ‘unlike’ the training data—with ‘unlike’ meaning everything from corrupted by noise to of a different semantic class all together (e.g. CIFAR-10 vs SVHN). We, on the other hand, are addressing *distributional shift*, which corresponds to making set or ‘batch’ level detections. This implies that even if $\tilde{\mathbf{X}}$ shares some elements with \mathbf{X} , $\tilde{\mathbf{X}}$ could still be considered OOD as we are comparing distributions. For example, take \mathbf{X} to be the set of MNIST digits and $\tilde{\mathbf{X}}$ the set of all 1s from MNIST. For large M , $\tilde{\mathbf{X}}$ would be considered atypical because a typical MNIST sample should not exhibit such as bias toward the 1-class. Operationally, there is another distinction in the ability to make per-instance decisions versus batch-wise decisions. The latter is in some ways easier since we can pool information across the set to inform the decision. When deploying a system involving neural networks, operating on batches of data is common practice as it amortizes communication overheads and makes GPU implementations more efficient. While our method works better as M increases, there are cases (e.g. train on SVHN, test on ImageNet) for which it can achieve near perfect OOD detection even when $M = 1$.

3 A Typicality Test for OOD Inputs

We now present a novel algorithm for detecting out-of-distribution inputs under the application setting described in the previous subsection: train set \mathbf{X} ($N > 50,000$), test set $\tilde{\mathbf{X}}$ ($M \geq 1$), decide if $\tilde{\mathbf{X}} \sim p^*$ or $\tilde{\mathbf{X}} \not\sim p^*$.² However, since we do not have access to p^* , we train a deep generative model on \mathbf{X} as a proxy. We assume that the model, denoted $p(\mathbf{x}; \theta)$ with parameters θ , is trained with maximum likelihood estimation (or via a lowerbound) and has a likelihood that can be evaluated (either directly or closely approximated). Examples of deep generative models that meet these specifications include normalizing flows [36] such as *Glow* [22], latent variable models such as *variational autoencoders* (VAEs) [23, 29], and auto-regressive models such as *PixelCNN* [38].

²A classic goodness-of-fit test would also be applicable here. We will discuss these tests and their limitations in a later section.

Under this model-based setting, we re-formulate the the OOD question as:

$$\text{if } \widetilde{\mathbf{X}} \in \mathcal{A}_\epsilon^M[p(\mathbf{x}; \boldsymbol{\theta})] \text{ then } \widetilde{\mathbf{X}} \sim p(\mathbf{x}; \boldsymbol{\theta}), \quad \text{otherwise } \widetilde{\mathbf{X}} \not\sim p(\mathbf{x}; \boldsymbol{\theta}). \quad (2)$$

In an ideal setting, we could mathematically derive the regions in \mathcal{X} that correspond to the typical set (e.g. the Gaussian’s annulus) and check if $\tilde{\mathbf{x}}$ resides within that region. Unfortunately, finding these regions is analytically intractable for neural-network-based generative models. To bypass this problem, we work directly with Shannon [33]’s entropy-based definition of typicality given in Definition 2.1. Using Equation 1, we can plug-in $\widetilde{\mathbf{X}}$ as a length M sequence and check if the ϵ -bound holds:

$$\text{if } \left| \frac{-1}{M} \sum_{m=1}^M \log p(\tilde{\mathbf{x}}_m; \boldsymbol{\theta}) - \mathbb{H}[p(\mathbf{x}; \boldsymbol{\theta})] \right| \leq \epsilon \text{ then } \widetilde{\mathbf{X}} \in \mathcal{A}_\epsilon^M[p(\mathbf{x}; \boldsymbol{\theta})]. \quad (3)$$

A practical implementation of Equation 3 requires the entropy $\mathbb{H}[p(\mathbf{x}; \boldsymbol{\theta})]$ and the threshold ϵ . We discuss computing $\mathbb{H}[p(\mathbf{x}; \boldsymbol{\theta})]$ first and then setting ϵ .

Monte Carlo Estimate of Entropy The entropy of the deep generative model is not available in closed-form and therefore we resort to the following sampling-based approximation. Recall from Subsection 2.1 that the AEP states that the sample entropy will converge to the true entropy as the number of samples grows. Since we have access to the model and can draw a large number of samples from it, the empirical entropy should be a good approximation for the true model entropy:

$$\mathbb{H}[p(\mathbf{x}; \boldsymbol{\theta})] = \int_{\mathcal{X}} p(\mathbf{x}; \boldsymbol{\theta})[-\log p(\mathbf{x}; \boldsymbol{\theta})]d\mathbf{x} \approx \frac{-1}{S} \sum_{s=1}^S \log p(\hat{\mathbf{x}}_s; \boldsymbol{\theta}) \quad (4)$$

where $\hat{\mathbf{x}}_s \sim p(\mathbf{x}; \boldsymbol{\theta})$. However, in preliminary experiments we observed markedly better OOD detection when using the training set \mathbf{X} instead of true samples from the model, i.e.

$$\mathbb{H}[p(\mathbf{x}; \boldsymbol{\theta})] \approx \int_{\mathcal{X}} p^*(\mathbf{x})[-\log p(\mathbf{x}; \boldsymbol{\theta})]d\mathbf{x} \approx \frac{-1}{N} \sum_{n=1}^N \log p(\mathbf{x}_n; \boldsymbol{\theta}). \quad (5)$$

This approximation should be good as well since we assume N to be large. We believe that the discrepancy in performance when using data vs samples is due to the deep generative models not representing p^* well enough. Indeed, we noticed only a slight degradation in performance on MNIST but severe degradation on ImageNet, thus supporting this conjecture. Improvements in generative modeling should allow samples from the model to be used in the future.

Final OOD Criterion Substituting the Monte Carlo entropy in Equation 5 into Equation 3 yields the final form for our OOD criterion:

$$\text{if } \left| \frac{-1}{M} \sum_{m=1}^M \log p(\tilde{\mathbf{x}}_m; \boldsymbol{\theta}) - \frac{-1}{N} \sum_{n=1}^N \log p(\mathbf{x}_n; \boldsymbol{\theta}) \right| \leq \epsilon \text{ then } \widetilde{\mathbf{X}} \in \mathcal{A}_\epsilon^M[p(\mathbf{x}; \boldsymbol{\theta})]. \quad (6)$$

Intuitively, Equation 6 is sensible in that it simply checks if the likelihood under $\widetilde{\mathbf{X}}$ is close to the likelihood under \mathbf{X} , the training set. This criterion is strictly stronger than previously proposed one-sided thresholds [6, 10] as it can reject points with either too low or too high of a density. We provide a sanity check for Equation 6 in Subfigure 1(c), showing the empirical value for ϵ calculated for the high-dimensional Gaussian example described in Section 2.1 (1000 samples from $\mathcal{N}(\mathbf{128}_{80 \times 80 \times 3}, \mathbb{I})$). We see that $\hat{\epsilon}$ achieves its minimum value exactly at \sqrt{d} -distance from $\mathbf{128}$.

Setting the OOD-Threshold with the Bootstrap We now turn to setting ϵ in Equation 6. We propose setting the OOD threshold through simulation—by constructing a (one-sided) *bootstrap confidence interval* (BCI) [15, 3] for the null hypothesis $H_0 : \widetilde{\mathbf{X}} \in \mathcal{A}_\epsilon^M[p(\mathbf{x}; \boldsymbol{\theta})]$, with the alternative being $H_1 : \widetilde{\mathbf{X}} \not\in \mathcal{A}_\epsilon^M[p(\mathbf{x}; \boldsymbol{\theta})]$. In a slight deviation from the tradition procedure for BCI construction, we assume the existence of a validation set \mathbf{X}' that was held-out from \mathbf{X} before training the generative model (just as is usually done for hyperparameter tuning).³ This is only to account for the generative

³Returning to the issue of using data vs samples, if the generative model could perfectly capture p^* , then the bootstrapping could be done with samples from the model instead of this validation set.

model overfitting to the training set. From this validation set, we bootstrap sample K ‘new’ data sets $\{\mathbf{X}'_k\}_{k=1}^K$ of size M and then plug each in to Equation 6 in place of $\tilde{\mathbf{X}}$:

$$\left| \frac{-1}{M} \sum_{m=1}^M \log p(\mathbf{x}'_{k,m}; \boldsymbol{\theta}) - \frac{-1}{N} \sum_{n=1}^N \log p(\mathbf{x}_n; \boldsymbol{\theta}) \right| = \hat{\epsilon}_k \quad (7)$$

where $\hat{\epsilon}_k$ is the estimate for the k bootstrap sample. All K estimates then form the bootstrap distribution

$$F(\epsilon) = \frac{1}{K} \sum_{k=1}^K \delta[\hat{\epsilon}_k]. \quad (8)$$

Calculating the α -quantile of $F(\epsilon)$, which we denote as ϵ_α^M , determines the threshold at which we reject the null hypothesis with confidence-level α [3]. If we reject the null, then we decide that the sample does not reside in the typical set and therefore is OOD. The complete procedure is summarized in Algorithm 1 in Appendix A. Observe that nearly all of the computation can be performed offline before any test set is received, including all bootstrap simulations. The rejection threshold ϵ_α^M depends on a particular M and α setting, but these computations can be done in parallel across multiple machines. The most expensive test-time operation is obtaining $\log p(\tilde{\mathbf{x}}, \boldsymbol{\theta})$. After this is done, only an $\mathcal{O}(M)$ operation to sum the likelihoods is required.

4 Related Work

Our work is directly motivated by the observations in Nalisnick et al. [26] and Choi et al. [8] that modern deep generative models can assign higher likelihood to OOD inputs. Our methodology is related to previous work on goodness-of-fit tests, using generative models for anomaly detection, and typicality in signal processing—all of which are well-studied areas. We summarize each below.

Statistical Tests The general problem of determining if a data set is drawn from a specific distribution is known as a *goodness-of-fit* (GoF) test [13, 20]. Many of the classical GoF tests rely on access to the cumulative distribution function (CDF) of interest and/or being able to compute an empirical distribution function (EDF) [12, 25, 2, 35]. These tests are not applicable to the deep generative models and high-dimensional data sets that we consider since CDFs and EDFs are both intractable in this setting. *Kernelized Stein discrepancy* [9, 24] is a recently-proposed GoF test that can scale to this regime and we compare against it in the experiments. When we have access to just samples from the reference distribution, this is known as a *two sample* GoF test. *Maximum mean discrepancy* [17] represents a scalable test of this class; we experimentally compare against it as well. There are several statistical tests for outliers [4], such as *Grubbs’s test* [18], but these usually rely on strong parametric assumptions or are restricted to univariate data.

Generative Models for Anomaly Detection When a proper statistical test cannot be applied, a related idea is to use a parametric model of the data to discover outliers and anomalies [28]. One of the most common techniques is to use a (one-sided) threshold on the density function to classify outliers [4]; this idea is used in Tarassenko et al. [37] Bishop [6], and Parra et al. [27], among others. Other work has applied more sophisticated techniques to density function evaluations to find outliers; for instance, Clifton et al. [10] applies extreme value theory. Yet this work and all others of which we are aware do not identify points with abnormally high density as anomalous. Thus they would fail in the settings presented by Nalisnick et al. [26]. As for work focusing on deep generative models in particular, most previous work proposes training improvements to make the model more robust. For instance, Hendrycks et al. [19] show that robustness and uncertainty quantification w.r.t. outliers can be improved by exposing the model to an auxiliary data set (a proxy for OOD data) during training. As for post-training outlier and OOD detection, Choi et al. [8] proposes using an ensemble of models to compute the *Watanabe-Akaike information criterion* (WAIC). However, there are no rigorous arguments for why WAIC should quantify GoF. Škvára et al. [34] proposes using a VAE’s conditional likelihood as an outlier criterion, finding that this works well only when the hyperparameters can be tuned using anomalous data. As far as we are aware, we are the first to apply a hypothesis testing framework to the problem of OOD or anomaly detection for deep generative models.

Typical Sets for Anomaly Detection Typical sets are a fundamental concept in data compression [11], but we are aware of only two previous works that use a notion of typicality for OOD, outlier, or anomaly detection. Sabeti and Høst-Madsen [31] propose a typicality framework based on minimum description length. They deem data as ‘atypical’ if it can be represented in less bits than one would expect under the generative model. While our frameworks share the same conceptual foundation, Sabeti and Høst-Madsen [31]’s implementation relies on strong parametric assumptions, is not based on entropy, and cannot be generalized to deep models (without drastic approximations). Choi et al. [8], the second work, leverages normalizing flows to test for typicality by transforming the data to a normal distribution and then deeming points outside the annulus to be anomalous. This approach restricts the generative model to be a Gaussian normalizing flow whereas ours is applicable to any generative model with a computable likelihood.

5 Experiments

We now evaluate our typicality test’s OOD detection abilities, focusing in particular on the image data set pairs highlighted by Nalisnick et al. [26]. We use the same three generative models as they did—Glow [22], PixelCNN [38], and Rosca et al. [30]’s VAE architecture—attempting to replicate training and evaluation as closely as possible. See Appendix B for a full description of model architectures and training. See Appendix C for more details on evaluation. We consider the following baselines; all statistical tests use $\alpha = 0.99$:

1. **t-test**: We apply a two-sample students’ t-test to check for a difference in means in the empirical likelihoods. In terms of Equation 6, this baseline will reject for any $\epsilon > 0$, and thus we expect it to be overly conservative. Moreover, this test does not have access to validation data and therefore improvements upon it can be attributed to our bootstrap procedure.
2. **Kolmogorov-Smirnov test (KS-test)**: We apply a two-sample KS-test to the likelihood EDFs. This test is stronger than our typicality test since it is checking for equivalence in all moments whereas ours (and the t-test) is restricted to the first moment. In turn, this test has a greater computational complexity— $\mathcal{O}(M \log M)$ compared to $\mathcal{O}(M)$.
3. **Maximum Mean Discrepancy (MMD)**: We apply a two-sample MMD [17] test to the data directly. Yet we incorporate the generative model by using a Fisher kernel [21]. We also apply the same bootstrap procedure on validation data to construct the test statistic. MMD has greater runtime still at $\mathcal{O}(NMd)$.
4. **Kernelized Stein Discrepancy (KSD)**: We apply KSD [24] to test for GoF to the generative model and again use a Fisher kernel and the bootstrap procedure on validation data. KSD has runtime $\mathcal{O}(M^2d)$. While we have ignored the construction of the kernel in the runtime analysis, KSD is the most costly due to having to take three derivatives through the model.
5. **Annulus Method**: We use a modified version of Choi et al. [8]’s annulus method applied to Gaussian normalizing flows. Like them, we classify something as OOD based on its distance to the sphere with radius \sqrt{d} . To make batch-wise decisions, we take the mean of the batch’s distances and reject the batch if this mean is greater than $d^{1/4}$ (for $\sigma = 1$). This baseline allows us to check for typicality directly in data-space.

5.1 Grayscale Images

We first evaluate our typicality test on grayscale images. We trained a Glow, PixelCNN, and VAE each on the FashionMNIST training split and tested OOD detection using the FashionMNIST, MNIST, and NotMNIST test splits. We use the FashionMNIST test split to evaluate for type-I error (incorrect rejection of the null) and the MNIST and NotMNIST splits for type-II error (incorrect rejection of the alternative). In Figure 2 we show the empirical distribution of likelihoods over each data set for each model. We see the same phenomenon as reported by Nalisnick et al. [26]—namely, that the MNIST OOD test set (green) has a higher likelihood than the training set (black). Lower-sided thresholding would clearly fail to detect the OOD sets. Table 1 reports a comparison against baselines, showing the fraction of M -sized batches classified as OOD. The IN-DIST. column reports the value for the FashionMNIST test set and ideally this number should be 0.00; any deviation from zero corresponds to type-I error. Conversely, the MNIST and NOTMNIST columns should be 1.00, and any deviation corresponds to type-II error. We see that for $M = 2$ all tests find it hard to reject the null hypothesis,

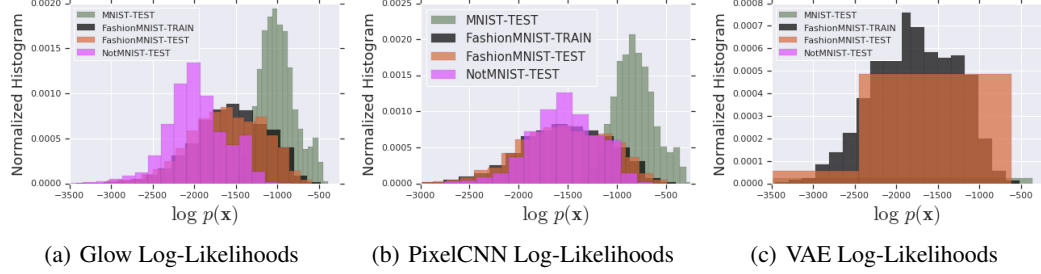


Figure 2: *Empirical Distribution of Likelihoods*. The above figure shows the histogram of log-likelihoods for FashionMNIST (train, test), MNIST (test), and NotMNIST (test) for the (a) Glow, (b) PixelCNN, and (c) VAE.

Table 1: *Grayscale Images: Fraction of Batches Classified as OOD*. The table below shows the fraction of M -sized batches rejected as OOD. The in-distribution column reflects type-I error and the MNIST and NotMNIST columns reflect type-II. The methods are ordered by their computational complexity.

METHOD	IN-DIST.	M = 2		M = 10		M = 25		
		MNIST	NOTMNIST	IN-DIST.	MNIST	NOTMNIST	IN-DIST.	MNIST
<i>Glow Trained on FashionMNIST</i>								
Typicality Test	0.02 \pm .01	0.14 \pm .10	0.08 \pm .04	0.02 \pm .02	1.00 \pm .00	0.69 \pm .11	0.01 \pm .00	1.00 \pm .00
<i>t</i> -Test	0.01 \pm .00	0.08 \pm .00	0.06 \pm .00	0.01 \pm .00	1.00 \pm .00	0.67 \pm .01	0.01 \pm .00	1.00 \pm .00
KS-Test	0.00 \pm .00	0.00 \pm .00	0.00 \pm .00	0.01 \pm .00	1.00 \pm .00	0.61 \pm .01	0.00 \pm .00	1.00 \pm .00
Max Mean Dis.	0.05 \pm .02	0.17 \pm .06	0.04 \pm .03	0.02 \pm .02	0.63 \pm .12	0.37 \pm .24	0.04 \pm .04	1.00 \pm .00
Kern. Stein Dis.	0.05 \pm .05	0.16 \pm .14	0.01 \pm .01	0.01 \pm .01	0.21 \pm .11	0.01 \pm .00	0.02 \pm .03	0.76 \pm .21
<i>PixelCNN Trained on FashionMNIST</i>								
Typicality Test	0.03 \pm .01	0.56 \pm .13	0.01 \pm .00	0.04 \pm .02	1.00 \pm .00	0.01 \pm .01	0.05 \pm .03	1.00 \pm .00
<i>t</i> -Test	0.01 \pm .00	0.23 \pm .00	0.00 \pm .00	0.01 \pm .00	1.00 \pm .00	0.00 \pm .00	0.02 \pm .00	1.00 \pm .00
KS-Test	0.00 \pm .00	0.00 \pm .00	0.00 \pm .00	0.02 \pm .00	1.00 \pm .00	0.00 \pm .00	0.04 \pm .00	1.00 \pm .00
Max Mean Dis.	0.02 \pm .00	0.03 \pm .01	0.36 \pm .05	0.05 \pm .02	0.27 \pm .06	1.00 \pm .00	0.06 \pm .04	0.59 \pm .10
Kern. Stein Dis.	0.01 \pm .00	0.05 \pm .02	0.08 \pm .03	0.02 \pm .01	0.29 \pm .14	0.61 \pm .20	0.05 \pm .02	0.70 \pm .11
<i>VAE Trained on FashionMNIST</i>								
Typicality Test	0.03 \pm .01	0.37 \pm .05	0.99 \pm .00	0.04 \pm .02	0.94 \pm .02	1.00 \pm .00	0.04 \pm .03	0.96 \pm .01
<i>t</i> -Test	0.01 \pm .00	0.20 \pm .00	0.99 \pm .00	0.02 \pm .00	0.93 \pm .00	1.00 \pm .00	0.02 \pm .00	0.96 \pm .00
KS-Test	0.00 \pm .00	0.00 \pm .00	0.00 \pm .00	0.02 \pm .00	1.00 \pm .00	0.00 \pm .00	0.02 \pm .00	1.00 \pm .00
Max Mean Dis.	0.03 \pm .02	0.16 \pm .07	0.73 \pm .01	0.03 \pm .04	0.41 \pm .16	1.00 \pm .00	0.01 \pm .01	0.64 \pm .05
Kern. Stein Dis.	0.04 \pm .01	0.05 \pm .01	0.74 \pm .00	0.11 \pm .04	0.17 \pm .01	1.00 \pm .00	0.06 \pm .04	0.37 \pm .03

which is not surprising given the overlap in the histograms in Figure 2. The exceptions are MNIST for the PixelCNN and NotMNIST for the VAE. Our typicality test (first row) is able to reject 56% of MNIST batches in the former case and 99% of batches in the latter case. One failure mode is on NotMNIST for the PixelCNN. None of the likelihood-based tests can distinguish NotMNIST as OOD due to the near perfect overlap in histograms shown in Figure 2(b). KSD and especially MMD are able to perform better in this case due to having access to the original feature-space representations (in addition to the generative model). Yet, surprisingly, KSD and MMD perform comparatively poorly for MNIST, especially at $M = 10$ and $M = 25$. We found the annulus method to be highly prone to type-I error and thus exclude it from the table. This agrees with the results reported by Choi et al. [8] that Gaussian normalizing flows do not necessarily make the latent space normally distributed.

5.2 Natural Images

We next turn to data sets of natural images—in particular SVHN, CIFAR-10, and ImageNet. We train Glow on SVHN, CIFAR-10, and ImageNet and use the two non-training sets for OOD evaluation. We found using MMD and KSD to be too expensive to make OOD decisions in an online system. Table 2 reports the fraction of M -sized batches classified as OOD. We see that our method (first row, bolded) is able to easily detect the OOD sets for SVHN, rejecting size-two batches at the rate of 98%+ while having only 1% type-I error. Performance on the CIFAR-10-trained model is good as well with 42%+ of OOD batches detected at $M = 2$ and 100% at $M = 10$ (type-I error at 1% in both cases). The hardest case is Glow trained on ImageNet: the KS-test performed best at $M = 25$.

with 89%, followed by the t- and typicality tests at 72% and 74% respectively. The annulus method was again quite poor, only being competitive in the easiest case of training on SVHN. We report additional results in Appendix D for our method, showing performance for all $M \in [1, 150]$ and when using CIFAR-100 as an OOD set.

Table 2: *Natural Images: Fraction of Batches Classified as OOD*. The table below shows the fraction of M -sized batches rejected as OOD.

METHOD	M = 2			M = 10			M = 25		
	SVHN	CIFAR-10	IMAGENET	SVHN	CIFAR-10	IMAGENET	SVHN	CIFAR-10	IMAGENET
<i>Glow Trained on SVHN</i>									
Typicality Test	0.01 \pm .00	0.98 \pm .00	1.00 \pm .00	0.00 \pm .00	1.00 \pm .00	1.00 \pm .00	0.02 \pm .00	1.00 \pm .00	1.00 \pm .00
<i>t</i> -Test	0.00 \pm .00	0.95 \pm .00	1.00 \pm .00	0.04 \pm .00	1.00 \pm .00	1.00 \pm .00	0.03 \pm .00	1.00 \pm .00	1.00 \pm .00
KS-Test	0.00 \pm .00	0.00 \pm .00	0.00 \pm .00	0.08 \pm .00	1.00 \pm .00	1.00 \pm .00	0.03 \pm .00	1.00 \pm .00	1.00 \pm .00
Annulus Method	0.12 \pm .00	0.45 \pm .00	1.00 \pm .00	0.00 \pm .00	0.54 \pm .00	1.00 \pm .00	0.00 \pm .00	0.59 \pm .00	1.00 \pm .00
<i>Glow Trained on CIFAR-10</i>									
Typicality Test	0.42 \pm .09	0.01 \pm .01	0.64 \pm .04	1.00 \pm .00	0.01 \pm .01	1.00 \pm .00	1.00 \pm .00	0.01 \pm .01	1.00 \pm .00
<i>t</i> -Test	0.44 \pm .01	0.01 \pm .00	0.65 \pm .00	1.00 \pm .00	0.02 \pm .00	1.00 \pm .00	1.00 \pm .00	0.02 \pm .00	1.00 \pm .00
KS-Test	0.00 \pm .00	0.00 \pm .00	0.00 \pm .00	1.00 \pm .00	0.01 \pm .00	0.98 \pm .00	1.00 \pm .00	0.01 \pm .00	1.00 \pm .00
Annulus Method	0.00 \pm .00	0.02 \pm .00	0.39 \pm .00	0.00 \pm .00	0.00 \pm .00	0.33 \pm .00	0.00 \pm .00	0.00 \pm .00	0.27 \pm .00
<i>Glow Trained on ImageNet</i>									
Typicality Test	0.78 \pm .08	0.02 \pm .01	0.01 \pm .00	1.00 \pm .00	0.20 \pm .06	0.01 \pm .01	1.00 \pm .00	0.74 \pm .05	0.01 \pm .01
<i>t</i> -Test	0.76 \pm .00	0.02 \pm .00	0.01 \pm .00	1.00 \pm .00	0.18 \pm .01	0.01 \pm .00	1.00 \pm .00	0.72 \pm .01	0.01 \pm .00
KS-Test	0.00 \pm .00	0.00 \pm .00	0.00 \pm .00	1.00 \pm .00	0.29 \pm .01	0.01 \pm .00	1.00 \pm .00	0.89 \pm .01	0.02 \pm .00
Annulus Method	0.00 \pm .00	0.02 \pm .00	0.01 \pm .00	0.00 \pm .00	0.00 \pm .00	0.00 \pm .00	0.00 \pm .00	0.00 \pm .00	0.00 \pm .00

Lastly, we report two challenging cases worthy of note and further attention. Figure 3(a) shows our method applied to Glow when trained on CIFAR-10, tested on CIFAR-100. The y -axis again shows fraction of batches reported as OOD and the x -axis the batch size M . Unsurprisingly given that CIFAR-10 is a subset of CIFAR-100, even at $M = 150$ our method classifies only 20% of batches as OOD. More interesting still is the case of Glow trained on CelebA, tested on CIFAR-10 and CIFAR-100. Figure 3(b) shows the histogram of log-likelihoods: all distributions peak at nearly the same value. The distribution of $\hat{\epsilon}$ observed during the bootstrap procedure ($M = 200$) is shown in Figure 3(c), with the red and black dotted lines denoting $\hat{\epsilon}$ computed using the whole set. We see that $\hat{\epsilon}$ for the OOD set is even less than the in-distribution’s, meaning that it would be impossible to reliably reject the OOD data while not rejecting the in-distribution test set as well.

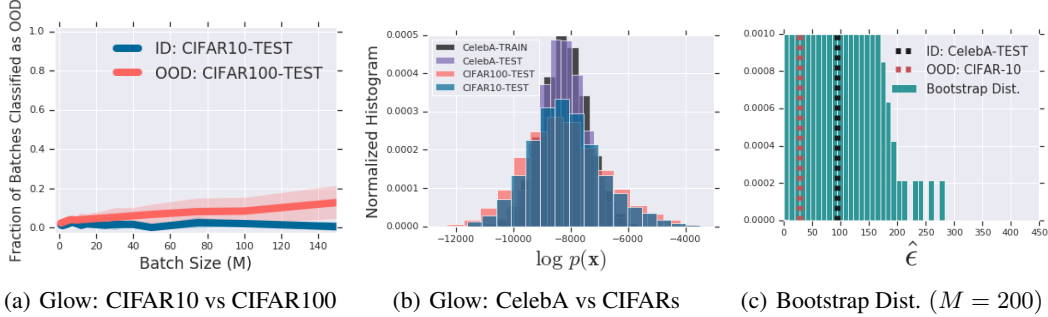


Figure 3: *Challenging Cases: CIFAR-10 vs CIFAR-100, CelebA vs CIFAR’s.*

6 Discussion and Conclusions

We have presented a model-agnostic and computationally efficient statistical test for OOD inputs derived from the concept of typical sets. In the experiments we showed that the proposed test is especially well-suited to deep generative models, identifying the OOD set for SVHN vs CIFAR-10 vs ImageNet [26] with high accuracy (while maintaining $\leq 1\%$ type-I error). In this work we used the null hypothesis $H_0 : \tilde{\mathbf{X}} \in \mathcal{A}_\epsilon^M$, which was necessary since we assumed access to only one training data set. One avenue for future work is to use auxiliary data sets [19] to construct a test statistic for the null $H_0 : \tilde{\mathbf{X}} \notin \mathcal{A}_\epsilon^M$, as would be proper for safety-critical applications. In our experiments we also noticed two cases—PixelCNN trained on FashionMNIST, tested on NotMNIST

and Glow trained on CelebA, tested on CIFAR—in which the empirical distributions of in- and out-of-distribution likelihoods matched near perfectly. Thus use of the likelihood distribution produced by deep generative models has a fundamental limitation that is seemingly worse than what was reported by Nalisnick et al. [26]. Aitchison et al. [1] showed that power-law data can give rise to a dispersed distribution of likelihoods, and thus examining connections between long-tailed data and typicality might explain this phenomenon.

References

- [1] Laurence Aitchison, Nicola Corradi, and Peter E Latham. Zipf’s Law Arises Naturally When There are Underlying, Unobserved Variables. *PLoS computational biology*, 12(12):e1005110, 2016.
- [2] Theodore W Anderson and Donald A Darling. A Test of Goodness of Fit. *Journal of the American statistical association*, 49(268):765–769, 1954.
- [3] Miguel A Arcones and Evarist Gine. On the Bootstrap of U and V Statistics. *The Annals of Statistics*, pages 655–674, 1992.
- [4] V. Barnett, P.S.V. Barnett, and T. Lewis. *Outliers in Statistical Data*. Wiley Series in Probability and Statistics. Wiley, 1994.
- [5] Michael Betancourt. A Conceptual Introduction to Hamiltonian Monte Carlo. *ArXiv e-print*, 2017.
- [6] Christopher M Bishop. Novelty Detection and Neural Network Validation. *IEE Proceedings-Vision, Image and Signal processing*, 141(4):217–222, 1994.
- [7] Varun Chandola, Arindam Banerjee, and Vipin Kumar. Anomaly Detection: A Survey. *ACM Computing Surveys*, 41(3):15, 2009.
- [8] Hyunsun Choi, Eric Jang, and Alexander Alemi. WAIC, but Why?: Generative Ensembles for Robust Anomaly Detection. *ArXiv e-Print arXiv:1810.01392v3*, 2019.
- [9] Kacper Chwialkowski, Heiko Strathmann, and Arthur Gretton. A Kernel Test of Goodness of Fit. In *International Conference on Machine Learning*, pages 2606–2615, 2016.
- [10] David A Clifton, Lei Clifton, Samuel Hugueny, and Lionel Tarassenko. Extending the Generalised Pareto Distribution for Novelty Detection in High-Dimensional Spaces. *Journal of Signal Processing Systems*, 74(3):323–339, 2014.
- [11] Thomas M Cover and Joy A Thomas. *Elements of Information Theory*. John Wiley & Sons, 2012.
- [12] Harald Cramér. On the Composition of Elementary Errors. *Scandinavian Actuarial Journal*, 1928(1):13–74, 1928.
- [13] Ralph B D’Agostino. *Goodness-of-Fit Techniques*, volume 68. CRC press, 1986.
- [14] Laurent Dinh, Jascha Sohl-Dickstein, and Samy Bengio. Density Estimation Using Real NVP. In *International Conference on Learning Representations (ICLR)*, 2017.
- [15] Bradley Efron. Bootstrap Methods: Another Look at the Jackknife. In *Breakthroughs in statistics*, pages 569–593. Springer, 1992.
- [16] Bradley Efron and Robert J Tibshirani. *An Introduction to the Bootstrap*. CRC press, 1994.
- [17] Arthur Gretton, Karsten M Borgwardt, Malte J Rasch, Bernhard Schölkopf, and Alexander Smola. A Kernel Two-Sample Test. *Journal of Machine Learning Research*, 13(Mar):723–773, 2012.
- [18] Frank E Grubbs. Procedures for Detecting Outlying Observations in Samples. *Technometrics*, 11(1):1–21, 1969.
- [19] Dan Hendrycks, Mantas Mazeika, and Thomas Dietterich. Deep Anomaly Detection with Outlier Exposure. In *International Conference on Learning Representations (ICLR)*, 2019.
- [20] Catherine Huber-Carol, Narayanaswamy Balakrishnan, M Nikulin, and M Mesbah. *Goodness-of-Fit Tests and Model Validity*. Springer Science & Business Media, 2012.
- [21] Tommi Jaakkola and David Haussler. Exploiting Generative Models in Discriminative Classifiers. In *Advances in Neural Information Processing Systems*, pages 487–493, 1999.

[22] Diederik P. Kingma and Prafulla Dhariwal. Glow: Generative Flow with Invertible 1x1 Convolutions. In *Advances in Neural Information Processing Systems (NeurIPS)*, 2018.

[23] Diederik P. Kingma and Max Welling. Auto-Encoding Variational Bayes. *International Conference on Learning Representations (ICLR)*, 2014.

[24] Qiang Liu, Jason Lee, and Michael Jordan. A Kernelized Stein Discrepancy for Goodness-of-Fit Tests. In *International Conference on Machine Learning*, pages 276–284, 2016.

[25] Frank J. Massey Jr. The Kolmogorov-Smirnov Test for Goodness of Fit. *Journal of the American Statistical Association*, 46(253):68–78, 1951.

[26] Eric Nalisnick, Akihiro Matsukawa, Yee Whye Teh, Dilan Gorur, and Balaji Lakshminarayanan. Do Deep Generative Models Know What They Don’t Know? In *International Conference on Learning Representations (ICLR)*, 2019.

[27] Lucas Parra, Gustavo Deco, and Stefan Miesbach. Statistical Independence and Novelty Detection with Information Preserving Nonlinear Maps. *Neural Computation*, 8(2):260–269, 1996.

[28] Marco AF Pimentel, David A Clifton, Lei Clifton, and Lionel Tarassenko. A Review of Novelty Detection. *Signal Processing*, 99:215–249, 2014.

[29] Danilo Rezende, Shakir Mohamed, and Daan Wierstra. Stochastic Backpropagation and Approximate Inference in Deep Generative Models. In *Proceedings of the 31st International Conference on Machine Learning (ICML)*, pages 1278–1286, 2014.

[30] Mihaela Rosca, Balaji Lakshminarayanan, and Shakir Mohamed. Distribution Matching in Variational Inference. *ArXiv e-Print arXiv:1802.06847*, 2018.

[31] Elyas Sabeti and Anders Høst-Madsen. Data Discovery and Anomaly Detection Using Atypicality for Real-Valued Data. *Entropy*, 21(3), 2019.

[32] Alireza Shafaei, Mark Schmidt, and James J. Little. Does Your Model Know the Digit 6 Is Not a Cat? A Less Biased Evaluation of “Outlier” Detectors. *ArXiv e-Print arXiv:1809.04729*, 2018.

[33] Claude Elwood Shannon. A Mathematical Theory of Communication. *Bell System Technical Journal*, 27(3):379–423, 1948.

[34] Vít Škvára, Tomáš Pevný, and Václav Šmídl. Are Generative Deep Models for Novelty Detection Truly Better? *KDD Workshop on Outlier Detection De-Constructed (ODD v5.0)*, 2018.

[35] Michael A. Stephens. EDF Statistics for Goodness of Fit and Some Comparisons. *Journal of the American Statistical Association*, 69(347):730–737, 1974.

[36] EG Tabak and Cristina V. Turner. A Family of Nonparametric Density Estimation Algorithms. *Communications on Pure and Applied Mathematics*, 66(2):145–164, 2013.

[37] L. Tarassenko, P. Hayton, N. Cerneaz, and M. Brady. Novelty Detection for the Identification of Masses in Mammograms. In *1995 Fourth International Conference on Artificial Neural Networks*, pages 442–447. IET, 1995.

[38] Aäron van den Oord, Nal Kalchbrenner, Lasse Espeholt, Oriol Vinyals, Alex Graves, et al. Conditional Image Generation with Pixel CNN Decoders. In *Advances in Neural Information Processing Systems (NeurIPS)*, 2016.

[39] Roman Vershynin. *High-Dimensional Probability: An Introduction with Applications in Data Science*, volume 47. Cambridge University Press, 2018.

Detecting Out-of-Distribution Inputs to Deep Generative Models Using a Test for Typicality: Appendix

A Algorithmic Implementation

Algorithm 1 A Bootstrap Test for Typicality

Input: Training data \mathbf{X} , validation data \mathbf{X}' , trained model $p(\mathbf{x}; \boldsymbol{\theta})$, number of bootstrap samples K , significance level α , M -sized batch of possibly OOD inputs $\tilde{\mathbf{X}}$.

Offline prior to deployment

1. **Compute** $\hat{\mathbb{H}}^N[p(\mathbf{x}; \boldsymbol{\theta})] = \frac{-1}{N} \sum_{n=1}^N \log p(\mathbf{x}_n; \boldsymbol{\theta})$.
2. **Sample** K M -sized data sets from \mathbf{X}' using bootstrap resampling.
3. **For all** $k \in [1, K]$:
 Compute $\hat{\epsilon}_k = \left| \frac{-1}{M} \sum_{m=1}^M \log p(\mathbf{x}'_{k,m}; \boldsymbol{\theta}) - \hat{\mathbb{H}}^N[p(\mathbf{x}; \boldsymbol{\theta})] \right|$ (Equation 7)
4. **Set** $\epsilon_\alpha^M = \text{quantile}(F(\epsilon), \alpha)$ (e.g. $\alpha = .99$)

Online during deployment

If $\left| \frac{-1}{M} \sum_{m=1}^M \log p(\tilde{\mathbf{x}}_m) - \hat{\mathbb{H}}^N[p(\mathbf{x}; \boldsymbol{\theta})] \right| > \epsilon_\alpha^M$:

Return $\tilde{\mathbf{X}}$ is out-of-distribution

Else:

Return $\tilde{\mathbf{X}}$ is in-distribution

B Generative Model Details

Glow Our *Glow* [22] implementation was derived from OpenAI’s open source repository⁴ and modified following the specifications in Appendix A of Nalisnick et al. [26]. All versions were trained with RMSProp, batch size of 32, with a learning rate of 1×10^{-5} for 100k steps and decayed by a factor of 2 after 80k and 90k steps. All priors were chosen to be standard Normal distributions. We follow Nalisnick et al. [26]’s zero-initialization strategy (last coupling layer set to zero) and in turn did not apply any normalization. Similarly, our convolutional layers were initialized by sampling from the same truncated Normal distribution [26]. For our FashionMNIST experiment, Glow had two blocks of 16 affine coupling layers (ACLs) [14]. The spatial dimension was only squeezed between blocks. For the SVHN, CIFAR-10, and ImageNet models, we used three blocks of 8 ACLs with multi-scale factorization occurring between each block. All ACL transformations used a three-layer highway network. 200 hidden units were used for fashionMNIST and 400 for all other data sets.

PixelCNN We trained a GatedPixelCNN [38] using Adam (1×10^{-4} initial learning rate, decayed by 1/3 at steps 80k and 90k, 100k total steps) for FashionMNIST and RMSProp (1×10^{-4} initial learning rate, decayed by 1/3 at steps 120k, 180k, and 195k, 200k total steps) for all other data sets. The FashionMNIST network had 5 gated layers (32 features) and a 256-sized skip connection. All other networks used 15 gated layers (128 features) and a 1024-sized skip connection

Variational Autoencoder We used the convolutional decoder VAE [23] variant described by Rosca et al. [30]. For Fashion MNIST, the decoder contained three convolutional layers with filter sizes 32, 32, and 256 and strides of 2, 2, and 1. Training was done again via RMSProp (1×10^{-4} initial learning rate, no decay, 200k total steps). For all other models, we followed the specifications in Rosca et al. [30] Appendix K.

⁴<https://github.com/openai/glow>

C Experimental Details

MMD and KSD Kernels We found that MMD and KSD only had good performance when using the Fisher kernel [21]: $k(\mathbf{x}_i, \mathbf{x}_j) = (\nabla_{\theta} \log p(\mathbf{x}_i; \theta))^T \nabla_{\theta} \log p(\mathbf{x}_j; \theta)$. All other kernels attempted required substantial tuning to the scale parameters and we did not want to assume access to enough data to perform this tuning. Furthermore, we found the memory cost of implementing the traditional Fisher kernel to be quite costly for Glow, each vector having 2million+ elements. Hence in the experiments we use the kernel modified such that the derivative is taken w.r.t. the input (making it the likelihood score): $k'(\mathbf{x}_i, \mathbf{x}_j) = (\nabla_{\mathbf{x}_i} \log p(\mathbf{x}_i; \theta))^T \nabla_{\mathbf{x}_j} \log p(\mathbf{x}_j; \theta)$.

Data Set Splits and Bootstrap Re-Samples For each data set we used the canonical train-test splits. To construct the validation set and perform bootstrapping, we extracted 5,000 samples from the test split and bootstrap sampled (with replacement) $K = 50$ data sets to calculate $F(\epsilon)$. We didn't find using $K > 50$ to markedly change performance. We then extracted another 5,000 samples from the test split, divided them into M -sized batches, and classified each other as OOD or not according to the various tests. We repeated this whole process 10 times, randomizing the instances in the validation and testing splits, in order to compute the means and standard deviations that are reported in Tables 1 and 2.

α -Level In preliminary experiments, we did not find a notable difference in type-II error when using $\alpha = 0.95$ vs $\alpha = 0.99$. Using the latter slightly improved type-I error and thus we used that value for all experiments and all methods.

D Additional Results: Varying M for Glow

Figure 4 reports results for our typicality test on Glow, varying M from $[1, 150]$. Table 2's results are a subset of these. We also report evaluations using CIFAR-100 as an OOD set.

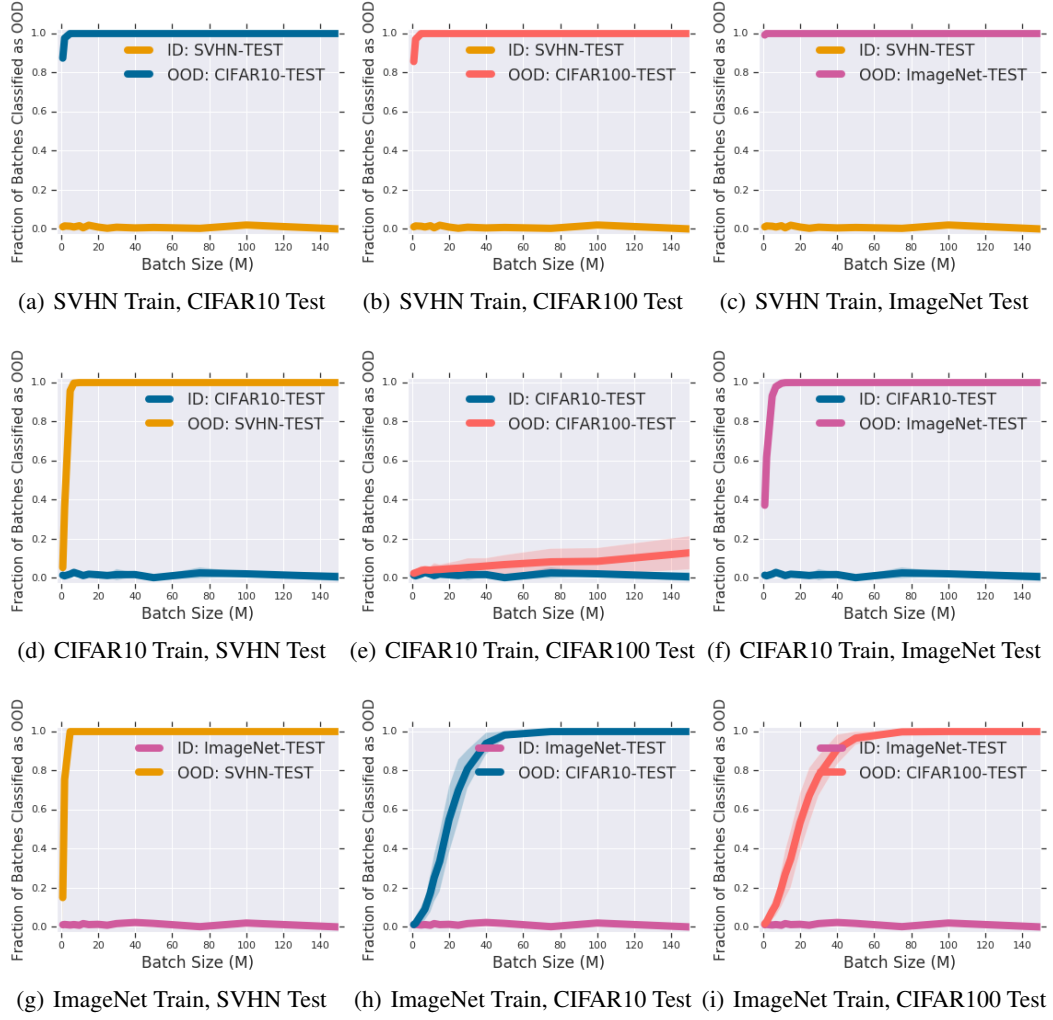


Figure 4: *Natural Image OOD Detection for Glow*. The above plots show the fraction of M -sized batches rejected for three Glow models trained on SVHN, CIFAR-10, and ImageNet. The OOD distribution data sets are these three training sets as well as CIFAR-100.